

# Binding of Bovine Serum Albumin to Heparin Determined by Turbidimetric Titration and Frontal Analysis Continuous Capillary Electrophoresis

Toshiaki Hattori,<sup>1</sup> Kozue Kimura, Emek Seyrek, and Paul L. Dubin<sup>2</sup>

*Department of Chemistry, Indiana University–Purdue University, Indianapolis, Indiana 46202*

Received October 23, 2000; published online July 19, 2001

**The association of proteins with glycosaminoglycans is a subject of growing interest, but few techniques exist for elucidating this interaction quantitatively. Here we demonstrate the application of capillary electrophoresis to the system of serum albumin (SA) and heparin (Hp). These two species form soluble complexes, the interaction increasing with reduction in pH and/or ionic strength (*I*). The acid–base property of Hp was characterized by potentiometric titration of ion-exchanged Hp. Conditions for complex formation with SA were qualitatively determined by turbidimetry, which revealed points of incipient binding ( $\text{pH}_i$ ) and phase separation ( $\text{pH}_\phi$ ), both of which depend on *I*. At  $\text{pH} > \text{pH}_\phi$ , i.e., prior to phase separation, frontal analysis continuous capillary electrophoresis was used to measure the concentration of free protein and to determine the protein–HP binding isotherm. The binding isotherms were well fit by the McGhee–von Hippel model to yield quantitative binding information in the form of intrinsic binding constants ( $K_{\text{obs}}$ ) and binding site size (*n*). The strong increase in  $K_{\text{obs}}$  with decrease of pH or *I* could be explained on the basis of electrostatic interactions, considering the effects of protein charge heterogeneity. The value of *n*, independent of pH, was rationalized on the basis of size considerations. The implications of these findings for clinical applications of Hp and for its physiological behavior are discussed. © 2001 Academic Press**

The binding of proteins to proteoglycans (PGs)<sup>3</sup> is an important biological phenomenon. For example, the interaction between chondroitin sulfate or keratan sulfate proteoglycans and collagen fibrils in the cartilage matrix defines the final shape of the tissue and provides the ability to withstand compressive load (1). Heparan sulfate proteoglycans (HSPGs) interact with fibronectin–collagen complexes in plasma membranes to assist cell adhesion (1). HSPGs in the glomerular basement membrane (GBM) also provide selective filtration of proteins (1, 2). These interactions appear to have a strong electrostatic component, arising from the interactions between charges on the proteins and the intense negative charge on glycosaminoglycans (GAGs) in PGs.

GAGs are highly diversified sulfated and carboxylated linear polysaccharides that constitute the major components of PGs. The backbone of the extracellular matrix PG aggregate is a high-molecular-weight (ca.  $2 \times 10^6$ ) hyaluronic acid, to which are bound a large number of core proteins; each core protein, in turn, is covalently bound to numerous GAGs (3–5). Many of the roles of PGs in extracellular signaling appear to depend on the interaction between GAGs and other macromolecules, in particular proteins (3, 6). Consequently, the study of GAG–protein interactions can facilitate a physical understanding of important biological phenomena.

Many techniques have been used to investigate the interaction between GAGs and proteins. For example, the formation of complexes has been detected using fluorescence (7, 8) and UV (8) absorption. Diffusion

<sup>1</sup> Current address: Research Center for Chemometrics, Toyohashi University of Technology, Toyohashi, Japan 441-8580.

<sup>2</sup> To whom correspondence should be addressed. Fax: (317) 274-6879. E-mail: [dubin@chem.iupui.edu](mailto:dubin@chem.iupui.edu).

<sup>3</sup> Abbreviations used: PGs, proteoglycans; HSPGs, heparin sulfate proteoglycans; GBM, glomerular basement membrane; GAGs, glycoaminoglycans; CE, capillary electrophoresis; Hp, heparin; FACCE, frontal analysis continuous capillary electrophoresis; BSA, bovine serum albumin; SEC, size-exclusion chromatography.

coefficients and sizes of complexes have been measured using light scattering (9, 10). Protein structural changes as a result of complexation between GAGs and proteins have been observed by circular dichroism measurement (CD) (11, 12) and NMR (13), and the binding sites of proteins and GAGs have been identified by X-ray crystallography of complexes between proteins and GAG oligomers (14). Complex mobilities have been measured by capillary electrophoresis (CE) (15).

Although numerous methods have been used to examine protein-GAG complexes, few techniques are capable of quantitatively determining an important variable: the GAG-protein complex formation constant. These potentiometric, spectroscopic, or chromatographic methods all pose respective difficulties. For example, the heparin(Hp)-protamine binding constant was determined using a Hp-sensitive electrode after neutralization of the complex (16), but the mechanism of this electrode response is not well understood, and other bulky anions e.g., free proteins of negative net charge, can act as interferents in this assay. Quantitation of complexation has been carried out using fluorescence (17-19), but this approach depends on a large change in absorption before and after complexation. While affinity chromatography has been used to measure the dissociation constant (20), large amounts of sample are required and the dissociation constant can be perturbed by the immobilization of protein or GAG.

Frontal analysis continuous capillary electrophoresis (FACCE) (21) is a new technique that has been demonstrated as a way to obtain precise and reliable binding data for protein-polyelectrolyte complexes. This technique resembles other capillary electrophoresis methods, namely the Hummel-Dreyer method, conventional frontal analysis method, affinity capillary electrophoresis, and vacancy peak and vacancy affinity capillary electrophoresis; however, each of these measurements of quantitative binding parameters poses some problems (22). Because the perturbation of the binding equilibria intrinsic to conventional frontal analysis method is overcome by continuous sampling, FACCE can be performed even when the mobility of the complex is not equal to the mobility of ligand or acceptor. Affinity capillary electrophoresis is useful for determining the dissociation constant of protein-Hp binding (23-26), but the resulting constant is not regarded as a true quantitative binding parameter when multiple ligands bind to the acceptor (22). On the other hand, FACCE may be used even in multiple complexation equilibria to measure the concentration of free ligand because its concentration is not determined from mobility; instead, the peak height directly indicates free ligand concentration. The stoichiometric relationship between bound li-

gand and the complex can then be fit to appropriate binding isotherms to yield binding constants and binding site size, two parameters that are very useful in elucidation of the binding mechanism. Moreover, sample requirements are smaller, and the measurement time is short. FACCE thus appears to be a simple, rapid, economical, precise, and reproducible method for quantitative characterization of protein-polyelectrolyte binding.

Previous studies with FACCE focused on combinations of proteins and synthetic polyelectrolytes (21). Here we are interested in developing FACCE methodology for combinations of proteins and biological polyelectrolytes. While the ultimate goal is to apply this technique to physiological cognates, our purpose here is to develop the methodology, as opposed to addressing a specific biochemical question. To do this, we have chosen bovine serum albumin (BSA) as the protein and heparin (Hp) as the biological polyelectrolyte.

The interaction of Hp and Hp-like GAGs with proteins is clearly of considerable interest. Hp-protein interactions regulate biological processes as diverse as complement activation, coagulation, cell adhesion, angiogenesis, platelet aggregation, lipolysis, and smooth muscle proliferation. Hp regulates angiogenesis, the growth of new capillary blood vessels, by interacting with peptide growth factors (27). It has an anticoagulant effect in coagulation, where binding to a plasma Hp cofactor is required for its activity (28); consequently, Hp is often used during surgical procedures or as an anticoagulant for thrombosis. Hp also has a direct aggregatory effect on platelets and lipoproteins; the interaction with the platelets causes platelet proaggregating and potentiating effects (29), while the binding of Hp to lipoprotein leads to aggregation or fusion of the lipoprotein during lipolysis (30). Hp is also responsible for the antiproliferative activity in smooth muscle proliferation (31). While these diverse and complex biological roles are not fully understood, they clearly involve the binding of many proteins.

Serum albumin is not a biochemical cognate of Hp, but it is the most abundant protein in the body and in particular is present at high concentration for intravenously administered Hp. Because the molecular weight of serum albumin is large (even in the absence of multimerization), complex formation of serum albumin with polymers is easily observed by many methods based on scattering or electrical mobility (32). The structure of serum albumin is well understood and its properties, particularly its ionization behavior, are thoroughly documented. Selection of the Hp/albumin pair as a demonstrative model of the quantitation of GAG-protein interactions using FACCE is thus based on numerous considerations.

## EXPERIMENTAL

### *Materials*

Heparin (sodium salt, porcine intestinal mucosa, Lot B27591), nominal  $M_r$  13,500–15,000 was from Calbiochem (La Jolla, CA). BSA (fatty acid free, Lot 8656224,  $M_r$  68,000) was purchased from Boehringer Mannheim Corp. (Indianapolis, IN). Analytical-grade dibasic sodium phosphate was obtained from J. T. Baker Chemical Co. (Phillipsburg, NJ) and monobasic sodium phosphate was from Mallinckrodt Inc. (Paris, KY). Other chemicals and reagents were obtained from current commercial sources at the highest level of purity available. All buffers and solutions were prepared with Milli-Q water (Millipore, Milford, MA).

### *Potentiometric Titration of Ion-Exchanged Hp*

Hp was ion-exchanged from the sodium salt to the hydrogen form using 45 ml of Dowex 50W-X8 (cation exchange resin; 5.1 meq/dry gram, 1.8 meq/ml resin bed) in a 50-ml buret column. A 10-ml solution containing 0.05 g of heparin sodium salt was poured into the column and washed through with Milli-Q water. After 10 ml of void volume was removed, at least 50 ml of solution was recovered. Collection of larger volumes did not increase the amount of measurable acid, proving that all the Hp was collected. The ion-exchanged Hp solution was titrated with 0.5 M NaOH using a Corning pH meter 240 with a FUTURA refillable combination pH electrode (Beckman, Fullerton, CA).

### *Turbidimetric Titration*

Turbidity measurements, reported as 100-%T, were performed at 420 nm using a Brinkman PC800 probe colorimeter equipped with a 1-cm path-length fiber optics probe. Turbidimetric titrations were carried out by adding 0.5 N HCl to mixed solutions of BSA (1 g/L) and Hp (0.1 g/L) containing variable concentrations of NaCl (0.01, 0.02, 0.05, 0.1, or 0.2 M NaCl). All titrations were carried out with gentle magnetic stirring, and the observed pH and transmittance were determined after the values had been stable for at least 1 min. The measured values were corrected by subtracting the turbidity of a Hp-free blank.

### *Frontal Analysis Continuous Capillary Electrophoresis*

Capillary electrophoresis was performed using a P/ACE 5500 CE (Beckman, Fullerton, CA) with UV detector, operating at 8 kV and 25°C. The fused silica capillary (Polymicro Technologies Inc., Phoenix, AZ) of dimensions 50  $\mu\text{m}$   $\times$  27 cm (effective length 20 cm) was prepared prior to each set of experiments by washing with 0.1 M NaOH for 10 min followed by a

10-min wash with Milli-Q water. This ensured a negative capillary surface charge under the experimental conditions.

Sample solutions were made from freshly prepared stock solutions of BSA and Hp dissolved in CE run buffer solution. The run buffer solution of  $I = 0.01$  consisted of disodium hydrogen phosphate and sodium dihydrogen phosphate adjusted to pH's 6.5, 6.8, and 7.0. The concentration range of BSA was 0.2–8.0 g/L and the concentration of Hp was constant at 0.2 g/L. The pH values of the samples were always adjusted to same pH as the run buffer.

The FACCE (21) experiment was initialized by equilibrating the capillary with buffer solution for 5 min. The inlet end of the capillary was then placed in a vial containing the equilibrated sample solution, and the outlet end was placed into a vial containing buffer solution. Constant voltage was applied, and separation, manifested in continuous plateaus, was observed. The first eluting plateau was the free protein, and the second was the free protein and the protein–Hp complex. Although a multiple peak pattern sometimes appeared instead of the second plateau, the first plateau was always obtained. After each electrophoretic run, a 5-min wash with 0.1 M NaOH followed by a 5-min rinse with water was performed. The concentration of free protein was determined from the height of first plateau, using a calibration curve constructed by measuring the plateau height of known concentrations of protein obtained under the same experimental conditions as for the protein–Hp mixture. The amount of bound BSA was obtained by subtracting the amount of measured free BSA from the total amount used.

### *Computational Methods*

Molecular modeling was done using DelPhi v98.0 (Molecular Simulations Inc.), where the electrostatic potential in and around the protein is calculated by nonlinear solution of Poisson–Boltzmann equation. The protein was placed in the center of a grid box with its largest dimension occupying 40% of the grid length. The resolution was set at 101 grid points per axis. The dielectric constants of the solvent and the protein were set to 80 and 2.5, respectively. Using the fractional charges for each charged amino acid residues, the electrostatic potential is then calculated at every point inside the grid box.

The charges of amino acid residues were determined using as a starting point the simple model put forward by Tanford (33). In this spherical-smear-charge model, the titration curve of a protein is a superposition of the curves for each of the seven groups of amino acids. The fraction  $\alpha$  of dissociated groups of any groups is given by

**TABLE 1**  
Intrinsic Dissociation Constants of Titratable Groups  
in BSA

| Type of group | Number<br>in group <sup>a</sup> | p <i>K</i> <sub>int</sub> <sup>a</sup> | Number<br>in group <sup>b</sup> | p <i>K</i> <sub>int</sub> <sup>c</sup> |
|---------------|---------------------------------|--|---------------------------------|--|
| β,γ-Carboxyl  | 99                              | 4.02                                   | 98                              | 4.1                                    |
| ε-Amino       | 57                              | 9.8                                    | 59                              | 10.3                                   |
| Imidazole     | 16                              | 6.9                                    | 16                              | 6.7                                    |
| Phenolic      | 19                              | 10.35                                  | 18                              | 11                                     |
| Guanidine     | 22                              | >12                                    | 24                              | 12                                     |
| α-Carboxyl    | 1                               | 3.75                                   | 1                               | 3.75                                   |
| α-Amino       | 1                               | 7.75                                   | 1                               | 7.75                                   |

<sup>a</sup> Values from Ref. (37).

<sup>b</sup> Actual number in group, taken from RCSB Protein Data Bank (crystal structure 1AO6).

<sup>c</sup> Best fit values (see text for explanation).

$$\text{pH} - \log\left(\frac{\alpha}{1 - \alpha}\right) = \text{p}K_{\text{int}} - \frac{1}{2.303kT} \frac{\partial W}{\partial Z}, \quad [1]$$

where  $K_{\text{int}}$  is an intrinsic dissociation constant characteristic of each group and  $W$  is the electrostatic free energy of the protein. All of the charges are considered to be smeared evenly over the surface so that positive and negative charges can cancel and only the average net charge  $\bar{Z}$  remains. The total electrostatic free energy is then the work of charging the sphere from zero to  $\bar{Z}$  and the work of charging due to the presence of the surrounding ions and is given by

$$W = \frac{\bar{Z}^2 \epsilon^2}{2D} \left( \frac{1}{b} - \frac{\kappa}{1 + \kappa a} \right), \quad [2]$$

where  $b$  is the radius of the sphere,  $a$  is the distance of closest approach between the centers of two ions (i.e.,  $a - b$  is the dimensions of a salt ion radius),  $\kappa$  is the Debye-Huckel parameter proportional to the square root of the ionic strength,  $\epsilon$  is the protonic charge, and  $D$  is the dielectric constant of the solvent. With this value of  $W$ , Eq. [1] becomes

$$\text{pH} - \log\left(\frac{\alpha}{1 - \alpha}\right) = \text{p}K_{\text{int}} - 0.868 w \bar{Z} \quad [3]$$

$$w = \frac{\epsilon^2}{2DkT} \left( \frac{1}{b} - \frac{\kappa}{1 + \kappa a} \right).$$

Equation [3] has been used extensively and successfully in the interpretation of potentiometric titrations studies of globular proteins such as ovalbumin, serum albumins, ribonuclease, hemoglobin, and β-lactoglobulin (34). Electrostatic interactions are thus accounted

for by  $0.868 w \bar{Z}$ , with  $w$  being essentially an empirical fitting parameter. Previous titration data of BSA could be well fit by Eq. [3] using ionic-strength-dependent  $w$  values (35). Titration curves were thus first constructed using these along with some  $w$  values interpolated with respect to ionic strength, in conjunction with  $\text{p}K_{\text{int}}$  values that represented approximately the mean of literature data (35). Then, the  $\text{p}K_{\text{int}}$  value for each group was adjusted in the range of previously found values until the differences between calculated and experimental titration curves were minimized at all ionic strengths. Adjusted  $\text{p}K_{\text{int}}$  values (see Table 1) were then used along with Eq. [3] to calculate the charges of each ionizable group at the desired pH and  $I$ .

## RESULTS AND DISCUSSION

### Potentiometric Titration of Ion-Exchanged Hp

Hp, a polydisperse polysaccharide consisting of several different disaccharide units, cannot be represented by any single structure (36). The contents of sulfate groups and carboxylate groups are thus variable and also dependent on the source (36). Since we find the binding between BSA and Hp to be mainly based upon electrostatic interaction, characterization of the ionic content of Hp is an important parameter which can formally be expressed by an equivalent weight (mass per unit charge group).

Figure 1 shows potentiometric titration curves of ion-exchanged Hp in the absence and presence of sodium chloride. The first inflection point must be the end point of the strong acid (sulfate and sulfamido) groups, and the second inflection that of the weak acids (carboxylate groups). The  $\text{p}K_a$  of the latter is elevated by the electrostatic influence of the strongly ionized groups. Consequently, the disappearance of the first

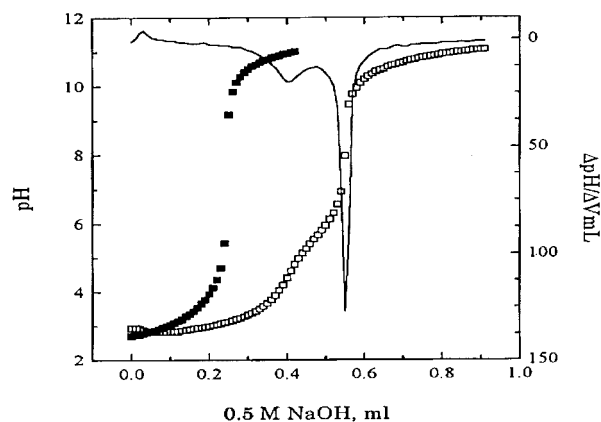


**FIG. 1.** Potentiometric titration of ion-exchanged heparin. (□) 0.0548 g of heparin in the absence of NaCl; (■) 0.0252 g of Hp in 1 M NaCl. Solid line is the differential of the titration curve without NaCl.

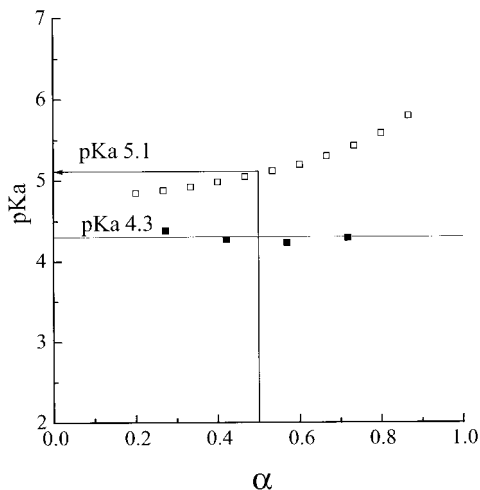


**FIG. 2.** The  $\alpha$  dependence of the  $pK_a$  of the carboxylate groups of heparin (□) in the absence of NaCl and (■) at  $I = 1.0$  M NaCl.

end point upon addition of 1 M sodium chloride is a result of the salt-induced depression of this  $pK_a$  so that the titration of the strong acid and carboxylate groups are no longer separable. The amount of NaOH consumed after the second end point is equivalent to the summation of the strong and weak acidic groups, so the equivalent weight was 5.0 meq/g. The relative ratio of carboxylate groups to strong acid groups was obtained as 1:2.7. This ratio corresponds to 2.7 sulfate and sulfonamide groups per disaccharide, in agreement with a literature value (14).

The dissociation constant of polycarboxylates such as poly(acrylic acid) in general depends on  $\alpha$  and  $I$  (37). Figure 2 shows the apparent dissociation constant,  $pK_a$  of the carboxylate groups, defined by  $pK_a = \text{pH} + \log[(1 - \alpha)/\alpha]$ , as a function of  $\alpha$  and  $I$ . In pure water,  $pK_a$  strongly depends upon  $\alpha$  and is larger than the intrinsic  $pK_a$ ; the value of  $pK_a$  is 5.1 at  $\alpha = 0.5$ , which agrees with the value of 5.1 measured by CD and potentiometric titration (38). This value is considerably larger than the  $pK_a$  of 3 determined by NMR (39). Possible limitations of the NMR method, particularly at concentrations as high as 10% w/v may be indicated by another report that the  $pK_a$  strongly decreases with Hp concentration (40), despite the fact that  $pK_a$ 's of polyacids are generally not reported to show strong concentration dependence. In any event, it is clear that intrinsic properties of polymer chains are best observed at high dilution, which can account for the good agreement between our value and the CD result, both measured at about 0.1% w/v. The addition of 1.0 M sodium chloride solution causes, as expected, a decrease in our measured  $pK_a$  from 5.1 to 4.3. This value is higher than  $pK_a = 3.28$  of D-glycopyranosyluronic acid (45) or the intrinsic dissociation constant,  $pK_0 = 2.9$ , of hyaluronic acid (46), indicating that the inhibi-

tion of the dissociation of carboxylate by the high negative charge of the sulfate groups persists even at high salt.

### Turbidimetric Titration

In order to establish appropriate conditions for FACCE, qualitative information about the binding of BSA–Hp is required. For a large protein such as BSA, turbidimetry is sufficiently sensitive to detect the soluble polyelectrolyte complex and so can be used to define three pH regions corresponding to no interaction, soluble complex, and precipitate or coacervate (38). Figure 3 shows the turbidimetric titration curve of the mixture of 1 g/L of BSA and 0.1 g/L of Hp in 0.03 M NaCl. In region 1, there is no complexation between BSA and Hp because of the strong coulombic repulsion between the net negatively charged BSA ( $pI \approx 4.9$ ) and the negatively charged Hp. In region 2, with decreasing negative charge, BSA forms a soluble complex with Hp. However, the soluble complex may form “on the wrong side” of  $pI$  (39), i.e., at  $\text{pH} > pI$ . The abrupt transition from region 1 to region 2, i.e., a well-defined “ $\text{pH}_c$ ” for soluble complex formation, can be verified by dynamic light scattering (39). In region 3, the complex aggregates and forms visible precipitate, with an abrupt increase in turbidity at “ $\text{pH}_\phi$ .” The dependences of  $\text{pH}_c$  and  $\text{pH}_\phi$  on  $I$  are shown as BSA–Hp “phase boundaries” in Fig. 4. Obviously, FACCE can only be done in region 2. The increase of  $I$  strongly depresses  $\text{pH}_c$ , since the salt screens electrostatic interactions, necessitating a larger protein positive charge. On the other hand,  $\text{pH}_\phi$  is independent of  $I$ , and this constant value is close to  $pI$  (38, 39).

### FACCE Electropherograms

In contrast to conventional frontal analysis, FACCE involves continuous sampling, so the electropherogram

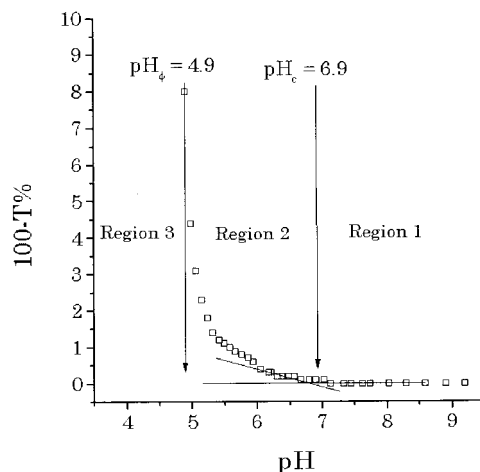


**FIG. 3.** Turbidimetric titration curve at  $I = 0.03$ , for 1 g/L of BSA with 0.1 g/L of heparin.

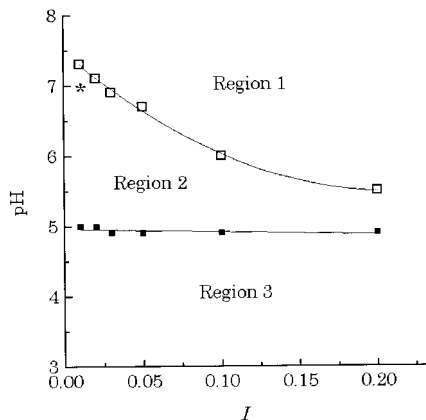


**FIG. 4.** Phase boundary for BSA (1 g/L) and heparin (0.1 g/L): (□) pH<sub>+</sub>; (■) pH<sub>-</sub>. (\*) point corresponding to conditions used for computational model in Fig. 8.

is a step-like separation profile, as shown in Fig. 5. Since the electrophoretic mobility of the complex is more negative than that of free BSA, the first plateau in the electropherogram is due to the elution of free BSA, and the second plateau is due to free BSA and complex. In conventional frontal analysis, the loss of free BSA in the mixture region (corresponding to second plateau) would make the complex decompose into free BSA and free Hp. In FACCE, however, the loss is made up by supplying free protein in the following eluent. The concentration of free BSA is equal and constant in both first and second plateaus and there is no perturbation of the binding equilibrium. The concentration of free BSA in the mixture of BSA and Hp is then determined by calibrating the peak height of first plateau.

An unexplained spike peak appears for Hp-free BSA, possibly due to limited adsorption of BSA onto the capillary. In order to minimize such adsorption FACCE was carried out only at pH > 6.5.

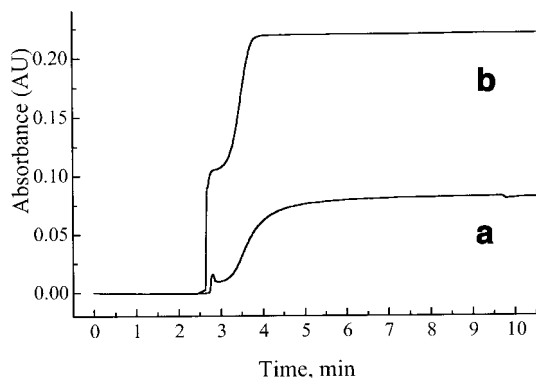


**FIG. 5.** Electropherograms obtained for (a) 1.0 g/L BSA + 0.2 g/L heparin, (b) 4.0 g/L BSA + 0.2 g/L heparin in phosphate buffer solution of  $I = 0.01$  at pH 6.5.

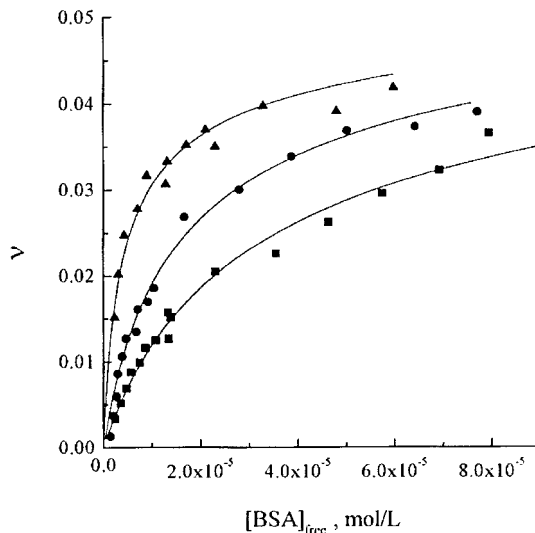


**FIG. 6.** Binding isotherms for BSA and heparin. (▲) pH 6.5; (●) pH 6.8; (■) pH 7.0; at  $I = 0.01$ .  $\nu$  is the number of bound BSA per negative heparin group.

### Binding Isotherms

Binding isotherms of BSA-Hp at  $I = 0.01$  M and at various pH values are shown in Fig. 6. Here  $[BSA]_{\text{free}}$  is the concentration of free BSA in the mixture, and  $\nu$  is the number of protein molecules bound per charged group.  $\nu$  is defined in this manner for the following reason. In the case of nonspecific binding arising from long-range electrostatic forces, the binding site does not correspond to a well-defined portion of the host macromolecule. The corresponding binding site size could be somewhat arbitrarily defined as a number of sugar rings or disaccharides. However, since the binding is primarily electrostatic, we choose here to discuss the size of the apparent binding site in terms of the number of charges it encompasses, a procedure similar to the one used in describing the binding of oligolysines to poly(rI) + poly(rU) (43). The relationship of  $\nu$ , the number of BSA bound per Hp charge group, to  $\nu^*$ , the number of BSA bound per disaccharide, is simply  $\nu^* = 3.7\nu$ .

The amount of BSA bound depends strongly on the pH. The diminution of the binding with pH must be the result of increased repulsion between Hp and BSA due to the increasing negative charge of BSA. The addition of salt also depresses the amount of BSA bound: even at  $I = 0.03$ , the concentration of BSA bound in pH 6.7 buffer solution was too low to obtain a significant result. These strong effects of pH and ionic strength indicate that the interaction is mainly due to coulombic forces between Hp and BSA.

The binding isotherms were fit to the McGhee-von Hippel (45) equation

$$v/L = K_{\text{obs}}(1 - nv) \left( \frac{1 - nv}{1 - (n-1)v} \right)^{n-1}, \quad [4]$$

where  $v$  is the number of bound BSA per ionic site of Hp,  $L$  is the concentration of free BSA,  $K_{\text{obs}}$  is the observed binding constant, and  $n$  is the number of binding sites. The two binding parameters of  $K_{\text{obs}}$  and  $n$  were obtained by nonlinear curve fitting of  $v/L$  vs  $v$ , and their values are listed in Table 2. Although the McGhee–von Hippel (MvH) model can be made to encompass cooperative binding (45), the binding isotherms in the present study were well fit without an additional cooperativity term. As shown by the solid lines in Fig. 6, the fitted curves conform very well to the experimental points. Similarly good two-parameter binding isotherm fits were reported for the binding between protein and synthetic polymers (46, 47). The intrinsic binding constant decreases strongly with increasing pH, while the binding site size expressed in terms of Hp ionic sites is  $n = 14$  independent of pH. This corresponds to a binding site size of 14/3.7 disaccharide units, i.e., an octasaccharide.

The binding isotherms in Fig. 6 may be converted into Fig. 7, which shows the number of BSA bound per disaccharide increasing with added BSA to a limiting value of 0.125. This corresponds to approximately three BSA bound per Hp molecule, based on an  $M_r$  of 14,000. The limiting value of 0.125 indicates that BSA occupies on average 8 disaccharides in Hp,  $N_{\text{lim}}$ , which is larger than the value  $N_{\text{site}} = 4$  found above; i.e., efficient packing in which every octasaccharide site is occupied does not occur. This result is consistent with the MvH “overlapping binding site” model, in which complete saturation of BSA is inhibited by the entropic resistance based on the “parking problem”: the binding possibilities for BSA depend upon the binding site of previously bound BSA. This effect, however, could also arise from the repulsive force between negatively charged neighboring bound proteins (see below) leading to anticooperative binding. Analysis of the binding isotherms does not make it possible to distinguish between these two types of anticooperativity. Since resolution between these two effects is not possible at the present time, the MvH plots should be recognized as effective empirical fits which, however, should not be

TABLE 2

Intrinsic Binding Constant and Binding Site Size of BSA–Hp at  $I = 0.01$  M

| pH  | $\log K_i$          | $n$                |
|-----|---------------------|--------------------|
| 6.5 | 4.12 ( $\pm 0.04$ ) | 15.5 ( $\pm 0.7$ ) |
| 6.8 | 3.56 ( $\pm 0.02$ ) | 13.9 ( $\pm 0.7$ ) |
| 7.0 | 3.23 ( $\pm 0.02$ ) | 13.7 ( $\pm 0.9$ ) |

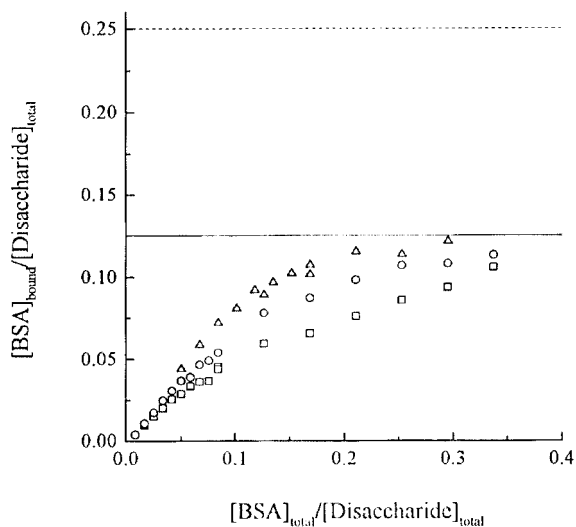


FIG. 7. Binding ratio of BSA per disaccharide of Hp. ( $\Delta$ ) pH 6.5; ( $\circ$ ) pH 6.8; ( $\square$ ) pH 7.0; all at  $I = 0.01$ . The solid line is at  $N_{\text{limit}} = 8$  and the dashed line is at  $N_{\text{site}} = 4$  (see text).

interpreted too rigidly. The fact that the MvH model is in principle strictly relevant to chains of infinite length (48) is a similar reason to avoid strict interpretation of the fitting parameters in terms of the theoretical model.

From  $N_{\text{site}} = 4$  and the length per disaccharide of ca. 1 nm (49), we can estimate that the contour length of the protein-binding site on Hp is about 4 nm, which is smaller than the Stokes diameter of BSA of ca. 7 nm (50). Thus, Hp does not wrap around BSA, but rather binds to some site on the protein, presumably a domain that bears a positive charge (see below). The consistency of  $n$  as a function of pH suggests constancy of the Hp-binding site of BSA; on the other hand, we find no evidence for a unique protein-binding site on Hp.

#### Computational Model of the Binding Site

The binding of a strong polyanion such as Hp to BSA at a pH well above  $pI$  indicates the presence of a positive “patch” in an otherwise negatively charged protein (44). Computer graphics allows us to identify one or more domains of positive potential, which must be involved in Hp binding by a protein of net negative charge, and also to visualize the implications of some of the results obtained from FACCE. However, if the potential was displayed on the protein surface, positive charges appeared in the negative domains and vice versa: no continuous and extensive positive potential domain could be observed. But when the potential was displayed 5 Å away from the van der Waals surface, positive and negative regions could clearly be distinguished. Figure 8 shows such an image of BSA, from three different views, for the conditions corresponding

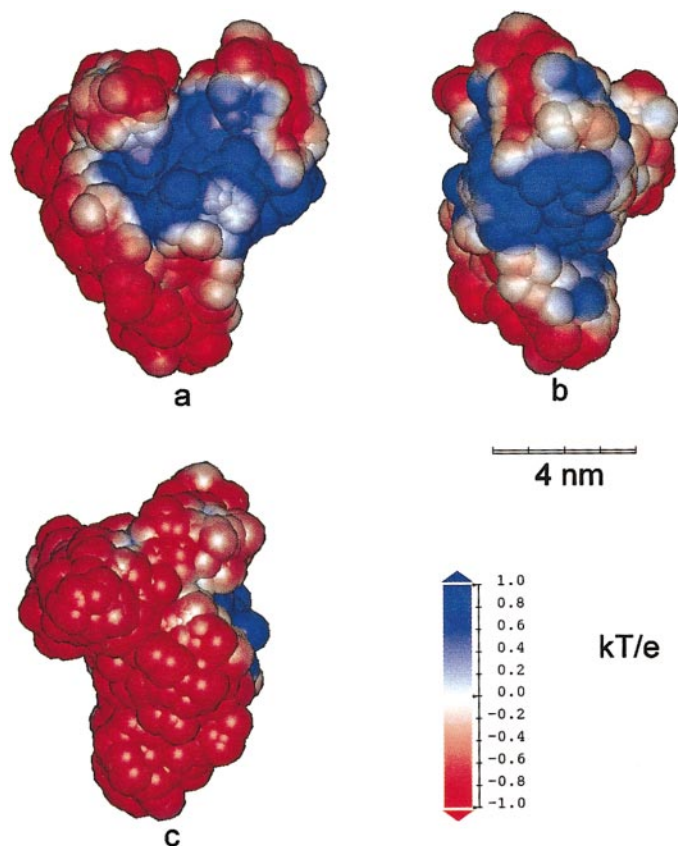


**FIG. 8.** (a) Electrostatic potential surface of BSA at 5 Å away from the van der Waals surface, under conditions of complex formation:  $I = 0.01$  and pH 7. (b) 90° rotated view of image in (a). (c) 270° rotated view of image in (a). The crystal structure of BSA (PDB ID: 1AO6) is taken from Research Collaboratory for Structure, Bioinformatics Protein Data Bank (<http://www.rcsb.org>) (57).

to the point represented by (\*) of Fig. 4 on the phase boundary in the region of complex formation (pH 7,  $I = 0.01$ ). The image in Fig. 8b shows a continuation of the positive potential patch in Fig. 8a.

As has been discussed earlier, Hp does not wrap around BSA, so the Hp-binding site is some portion of this patch, corresponding—as discussed above—to a size of about 4 nm, consistent with the view in Fig. 8b. The modest curvature of this site is in accord with the flexibility of the Hp molecules. The side of the protein opposite to the binding side shown in Fig. 8c is strongly negative. Thus, repulsive interactions among bound BSA could lead to anticooperative binding.

The binding of Hp to protein cognates has been discussed in terms of specific amino acid sequences that constitute the Hp-binding site(s) (14). This description of specific binding differs fundamentally from loose nonspecific binding at the 5-Å surface proposed here for BSA and Hp. In our model multiple configurations of the Hp chain which approximate the minimum energy state may exist. Whether such a model is tenable

for glycosaminoglycan–protein pairs will be the subject of future investigations.

### Physiological and Clinical Implications

The present results may be relevant to some of the clinical applications of Hp, as well as its physiological functions. Hp has been administered as a treatment for albuminuria (abnormal urinary excretion of albumin) (51, 52) in diabetics. It has been suggested that albuminuria, which is a loss of filtration selectivity in the glomerular basement membrane GBM, could arise from a diminution of the heparin sulfate proteoglycan content of the GBM (53), consequently, albumin-free filtration might be restored if Hp were to somehow ameliorate this loss. Figure 4 shows that physiological blood conditions (pH 7.4,  $I = 0.15$  M) correspond to strong repulsive interactions between BSA and Hp, even under acidosis or hyponatremia (the decrease of sodium concentration in blood), and Hp as a component of the GBM should reduce serum albumin filtration. On the other hand, severe reduction of  $I$  can lead to attraction (region 2 or 3 in Fig. 4).  $I$  values as low as 40 mM have been suggested for cartilage because of the ionic exclusion properties of proteoglycans (54). In osteoarthritic cartilage, in which Hp has been found to constitute 3–4% of proteoglycans (55), the amount of albumin increases significantly (56). In such tissues, attractive serum albumin–Hp interactions may exist.

### ACKNOWLEDGMENTS

This research was supported by NSF Grant CHE-9987891. The authors thank Kristopher Grymonpré for his help with molecular modeling.

### REFERENCES

1. Rhoades, R., and Pflanzner, R. (1996) Human Physiology, 3rd ed., pp. 704–735, Saunders College, Orlando.
2. Farquhar, M. G. (1985) The glomerular basement membrane: A selective macromolecular filter. *In* Cell Biology of the Extracellular Matrix (Hay, E. D., Ed.), pp. 335–378, Plenum, New York.
3. Sames, K. (1994) The Role of Proteoglycans and Glycosaminoglycans in Aging, Karger, Basel.
4. Dannell, J., Lodish, H., and Baltimore, D. (1990) Molecular Cell Biology, Chap. 23, Freeman, New York.
5. Jackson, R. L., Busch, S. J., and Cardin, A. D. (1991) Glycosaminoglycans: Molecular properties, protein interactions, and role in physiological processes. *Physiol. Rev.* **71**, 481–539.
6. Kjellen, L., and Lindahl, U. (1991) Proteoglycans: Structures and interactions. *Annu. Rev. Biochem.* **60**, 443–475.
7. Teramoto, A., Takagi, Y., Hachimori, A., and Abe, K. (1999) Interaction of albumin with polysaccharides containing ionic groups. *Polym. Adv. Technol.* **10**, 681–686.
8. Finotti, P., and Pagetta, A. (1997) Heparin-induced structural modifications and oxidative cleavage of human serum albumin in the absence and presence of glucose: Implications for transcapillary leakage of albumin in hyperglycaemia. *Eur. J. Biochem.* **247**, 1000–1008.

9. Eigner, W., Mitterer, A., Schurz, J., and Günther, J. (1982) Light-scattering investigations on LDL-heparin complexes. *Bio-sci. Rep.* **2**, 413–417.
10. Mach, H., Volkin, D. B., Burke, C. J., and Middaugh, R. (1993) Nature of the interaction of heparin with acidic fibroblast growth factor. *Biochemistry* **32**, 5480–5489.
11. Lima, L. T. R., and De Prat-Gay, G. (1997) Conformational changes and stabilization induced by ligand binding in the DNA-binding domain of the E2 protein from human papillomavirus. *J. Biol. Chem.* **272**, 19295–19303.
12. Vyas, A. A., Pan, J., Patel, H. V., Vyas, K. A., Chiang, C., Sheu, Y., Hwang, J., and Wu, W. (1997) Analysis of binding of cobra cardiotoxins to heparin reveals a new  $\beta$ -sheet heparin-binding structural motif. *J. Biol. Chem.* **272**, 9661–9670.
13. Pineda-Lucena, A., Jiménez, M. A., Lozano, R. M., Nieto, J. L., Santoro, J., Rico, M., and Giménez-Gallego, G. (1996) Three-dimensional structure of acidic fibroblast growth factor in solution: Effects of binding to a heparin functional analog. *J. Mol. Biol.* **264**, 162–178.
14. Hileman, R. E., Fromm, J. R., Weiler, J. M., and Linhardt, R. J. (1998) Glycosaminoglycan-protein interaction: Definition of consensus sites in glycosaminoglycan binding proteins. *BioEssay* **20**, 156–167.
15. Gunnarsson, K., Valtcheva, L., and Hjertén, S. (1997) Capillary zone electrophoresis for the study of the binding of antithrombin to low-affinity heparin. *Glycoconjugate J.* **14**, 859–862.
16. Ramamurthy, N., Baliga, N., Wakefield, T. W., Andrews, P. C., Yang, V. C., and Meyerhoff, M. E. (1999) Determination of low-molecular-weight heparins and their binding to protamine and a protamine analog using polyion-sensitive membrane electrodes. *Anal. Biochem.* **266**, 116–124.
17. Crescenzi, V., Rizzo, R., and Manzini, G. (1981) Model system studies of polysaccharide-proteins interactions. *Period. Biol.* **83**, 31–38.
18. Patel, H. V., Vyas, A. A., Vyas, K. A., Liu, Y., Chiang, C., Chi, L., and Wu, W. (1997) Heparin and heparan sulfate bind to snake cardiotoxin. *J. Biol. Chem.* **272**, 1484–1492.
19. Olson, S. T., Halvorson, H. R., and Bjork, J. (1991) Quantitative characterization of the thrombin-heparin interaction. *J. Biol. Chem.* **266**, 6342–6352.
20. Maccarana, M., and Lindahl, U. (1997) Mode of interaction between platelet factor 4 and heparin. *Glycobiology* **3**, 271–277.
21. Gao, J. Y., Dubin, P. L., and Muhoberac, B. B. (1997) Measurement of the binding of proteins to polyelectrolytes by frontal analysis continuous capillary electrophoresis. *Anal. Chem.* **69**, 2945–2951.
22. Busch, M. H. A., and Kraak, H. P. (1997) Principles and limitations of methods available for the determination of binding constants with affinity capillary electrophoresis. *J. Chromatogr. A.* **777**, 329–353.
23. Gunnarsson, K., Valtcheva, L., and Hjertén, S. (1997) Capillary zone electrophoresis for the study of the binding of antithrombin to low-affinity heparin. *Glycoconjugate J.* **14**, 859–862.
24. Heegaard, N. H. H. (1998) A heparin-binding peptide from human serum amyloid P component characterized by affinity capillary electrophoresis. *Electrophoresis* **19**, 442–447.
25. VanderNoot, V. A., Hileman, R. E., Dordick, J. S., and Linhardt, R. J. (1998) Affinity capillary electrophoresis employing immobilized glycosaminoglycan to resolve heparin-binding peptides. *Electrophoresis* **19**, 437–441.
26. Wu, X., and Linhardt, R. J. (1998) Capillary affinity chromatography and affinity capillary electrophoresis of heparin binding proteins. *Electrophoresis* **19**, 2650–2653.
27. Folkman, J., and Shing, Y. (1992) Control of angiogenesis by heparin and other sulfated polysaccharides. *Adv. Exp. Med. Biol.* **313**, 355–364.
28. Hirsh, J., and Fuster, V. (1994) Guide to anticoagulant-therapy. I. Heparin. *Circulation* **89**, 1449–1466.
29. Burgess, J. K., and Chong, B. H. (1997) The platelet proaggregating and potentiating effects of unfractionated heparin, low molecular weight heparin and heparinoid in intensive care patients and healthy controls. *Eur. J. Haematology* **58**, 279–285.
30. Hakala, J. K., Oorni, K., Ala-Korpela, M., and Kovanen, P. T. (1999) Lipolytic modification of LDL by phospholipase A(2) induces particle aggregation in the absence and fusion in the presence of heparin. *Arterioscler Thromb. Vasc. Biol.* **19**, 1276–1283.
31. Garg, H. G., Joseph, P. A. M., Thompson, B. T., Hales, C. A., Toida, T., Imanari, T., Capila, I., and Linhardt, R. J. (1999) Effect of fully sulfated glycosaminoglycans on pulmonary artery smooth muscle cell proliferation. *Arch. Biochem. Biophys.* **371**, 228–233.
32. Gao, J. Y., Dubin, P. L., and Muhoberac, B. B. (1998) Capillary electrophoresis and dynamic light scattering studies of structure and binding characteristics of protein-polyelectrolyte complexes. *J. Phys. Chem. B* **102**, 5529–5535.
33. Tanford, B. C., and Kirkwood, J. G. (1957) Theory of protein titration curves. I. General equations for impenetrable spheres. *J. Am. Chem. Soc.* **79**, 5333–5339.
34. Edsall, J., and Wyman, J. (1958) *Biophysical Chemistry*, Academic Press, New York, NY.
35. Tanford, C., Swanson, S. A., Shore, W. S. (1955) Hydrogen ion equilibria of bovine serum albumin. *J. Am. Chem. Soc.* **77**, 6414–6421.
36. Casu, B. (1985) Structure and biological activity of heparin. *Adv. Carbohydr. Chem. Biochem.* **43**, 51–134.
37. Nagasawa, M., Murase, T., and Kondo, K. (1965) Potentiometric titration of stereoregulator polyelectrolytes. *J. Phys. Chem.* **69**, 4005–4012.
38. Park, J. W., and Chakrabarti, B. (1977) Acid-base and optical properties of heparin. *Biochem. Biophys. Res. Commun.* **78**, 604–608.
39. Wang, H., Loganathan, D., and Linhardt, R. J. (1991) Determination of the  $pK_a$  of glucuronic acid and the carboxy groups of heparin by  $^{13}\text{C}$ -nuclear-magnetic resonance spectroscopy. *Biochem. J.* **278**, 689–695.
40. Gatti, G., Casu, B., Hamer, G. K., and Perlin, A. S. (1979) Studies on the conformation of heparin by  $^1\text{H}$  and  $^{13}\text{C}$  NMR spectroscopy. *Macromolecules* **12**, 1001–1007.
41. Kohn, R., and Kovac, P. (1978) Dissociation constants of D-galacturonic and D-glucuronic acid and their O-methyl derivatives. *Chem. Zvesti* **32**, 478–485.
42. Cleland, R. L., Wang, J. L., and Detweiler, D. M. (1982) Polyelectrolyte properties of sodium hyaluronate. 2. Potentiometric titration of hyaluronic acid. *Macromolecules* **15**, 386–395.
43. Mattison, K. W., Brittain, I. J., and Dubin, P. L. (1995) Protein-polyelectrolyte phase boundaries. *Biotech. Prog.* **11**, 632–637.
44. Park, J. M., Muhoberac, B. B., Dubin, P. L., and Xia, J. (1992) Effect of protein charge heterogeneity in protein-polyelectrolyte complexation. *Macromolecules* **25**, 290–295.
45. McGhee, J. D., and von Hippel, P. H. (1974) Theoretical aspects of DNA-protein interaction: Co-operative and non-co-operative binding of large ligands to a one-dimensional homogeneous lattice. *J. Mol. Biol.* **86**, 469–489.

46. Hallberg, R. K., and Dubin, P. L. (1998) Effects of pH on the binding of  $\beta$ -lactoglobulin to sodium polystyrene sulfonate. *J. Phys. Chem. B* **102**, 8629–8633.
47. Hattori, T., Hallberg, R. K., and Dubin, P. L. (2000) Roles of electrostatic interaction and polymer structure in the binding of  $\beta$ -lactoglobulin to anionic polyelectrolytes: Measurement of binding constants by frontal analysis continuous capillary electrophoresis. *Langmuir* **16**, 9738–9743.
48. Epstein, I. R. (1978) Cooperative and noncooperative binding of large ligands to a finite one-dimensional lattice: A model for ligand–oligonucleotide interactions. *Biophys. Chem.* **8**, 327–339.
49. Comper, W. D., and Laurent, T. C. (1978) Physiological function of connective tissue polysaccharides. *Physiol. Rev.* **58**, 255–315.
50. Kronman, M. J., and Foster, J. F. (1957) Sedimentation and optical rotation behavior of bovine plasma albumin at low pH in presence of various anions: Effect of charge on molecular expansion. *Arch. Biochem. Biophys.* **72**, 205–218.
51. Gambaro, G., Cavazzana, A. O., Luzi, P., Piccooli, A., Borsatti, A., Crepaldi, G., Marchi, E., and Venturini, A. P. (1992) Glycosaminoglycans prevent morphological renal alterations and albuminuria in diabetic rats. *Kidney Int.* **42**, 285–291.
52. Myrup, B., Hansen, P. M., Jensen, T., Kofoed-Enevoldsen, A., Feldt-Rasmussen, B., Gram, J., Kluff, C., Jespersen, J., and Deckert, T. (1995) Effect of low-dose heparin on urinary albumin excretion in insulin-dependent diabetes mellitus. *Lancet* **345**, 421–422.
53. Yokoyama, H., Høyer, P. E., Hansen, P. M., van den Born, J., Jensen, T., Berden, J. H. M., Deckert, T., and Garbarsch, C. (1997) Immunohistochemical quantification of heparan sulfate proteoglycan and collagen IV in skeletal muscle capillary basement membrane of patients with diabetic nephropathy. *Diabetes* **46**, 1875–1880.
54. Urban, J., and Hall, A. (1992) Physical modifiers of cartilage metabolism. *in* Articular Cartilage and Osteoarthritis (Kuettner, K., *et al.*, Eds.), pp. 393–409, Raven Press, New York.
55. Yusipova, N. A., and Kriuk, A. S. (1979) Articular cartilage, blood serum glycosaminoglycans, and glycoproteins in osteoarthritis deformans. *Clin. Chim. Acta* **94**, 9–21.
56. Vilamitjana-Amédée, J., and Harmand, M. F. (1990) Biochemical analysis of normal and osteoarthritic human cartilage. *Clin. Physiol. Biochem.* **8**, 221–230.
57. Carter, D. C., and Mo, J. X. (1994) Structure of serum albumin, *Adv. Protein Chem.* **45**, 153–158.